

# Unconventional four-terminal thermoelectric transport due to inelastic transport: Cooling by transverse heat current, transverse thermoelectric effect, and Maxwell demon

Jincheng Lu<sup>1</sup>, Jian-Hua Jiang<sup>1,\*</sup> and Yoseph Imry<sup>2,†</sup>

<sup>1</sup>*School of Physical Science and Technology, and Collaborative Innovation Center of Suzhou Nano Science and Technology, Soochow University, Suzhou 215006, China*

<sup>2</sup>*Department of Condensed Matter Physics, Weizmann Institute of Science, Rehovot 76100, Israel*



(Received 13 August 2020; revised 1 February 2021; accepted 3 February 2021; published 19 February 2021)

We show that, in mesoscopic four-terminal thermoelectric devices with two electrodes (the source and the drain) and two heat baths, inelastic-scattering processes can lead to unconventional thermoelectric transport. The source (or the drain) can be cooled by passing a thermal current between the two heat baths, with no net heat exchange between the heat baths and the electrodes. This effect, termed “cooling by transverse heat current,” is a mesoscopic heat drag effect. In addition, there is a transverse thermoelectric effect where electrical current and power can be generated by a transverse temperature bias (i.e., the temperature bias between the two heat baths). This transverse thermoelectric effect originates from inelastic-scattering processes and may have advantages for improved figures of merit and power factor due to spatial separation of charge and heat transport. We study the Onsager current-affinity relations, the linear-response transport properties, and the transverse thermoelectric figure of merit of the four-terminal thermoelectric devices for various system parameters. We find that the figures of merit are optimized in different parameter regions for the transverse and the (conventional) longitudinal thermoelectric effects, respectively. Meanwhile, the maximum figure of merit for the transverse thermoelectric effect is higher than the figure of merit for the conventional longitudinal thermoelectric effect. In addition, we investigate the efficiency and power of the cooling by the transverse heat current effect in both linear and nonlinear transport regimes. Finally, we demonstrate that, by exploiting the inelastic transport in the quantum-dot four-terminal systems, a type of Maxwell demon can be realized using nonequilibrium heat baths.

DOI: [10.1103/PhysRevB.103.085429](https://doi.org/10.1103/PhysRevB.103.085429)

## I. INTRODUCTION

The study of thermoelectric transport on the nanoscale [1–5] is important for at least two reasons. First, it is a realm where mesoscopic fluctuations and dissipations work together with quantum mechanics [6–19]. Second, nanostructured materials are important routes toward high thermoelectric efficiency and power, as motivated by the seminal works of Hicks and Dresselhaus [20–23]. While most of the studies are based on elastic transport processes, recent researches found that inelastic transport processes lead to phenomena that have not been found in elastic transport [8,17,24–33]. The first example is the cooling by heating effect in three-terminal (i.e., two electronic electrodes and a bosonic terminal) thermoelectric transport where one of the two electronic reservoirs can be cooled (the other one heated) by heat injection from the bosonic reservoir [34–36]. The second example is the linear thermal transistor effect, namely, that using the three-terminal inelastic thermoelectric transport thermal transistor effect can be realized in the linear-response regime without relying on nonlinear negative differential thermal conductance [30,37].

Inelastic thermoelectric transport realizes high-efficiency and powerful thermoelectric devices. As shown in Refs. [26] and [38], high figure of merit inelastic thermoelectric de-

vice requires only small bandwidth of the bosons involved in the inelastic processes. Unlike Mahan and Sofo’s proposal of using narrow electronic bandwidth [39], such a requirement does not cause suppressed electrical conductivity and power [29,40,41], if the interaction between electrons and bosons are strong. Such inelastic thermoelectric devices can have large figures of merit and high power factors. It was found recently by Whitney *et al.* [42] that, in four-terminal thermoelectric transport through a quantum dot (QD; i.e., the source, the drain, and the two electrodes that are capacitively coupled with the QD as two thermal baths), electrical power can be generated even when the total heat injection from the two thermal baths vanishes. Such unconventional thermoelectric conversion is realized through mesoscopic Coulomb drag, which is an inelastic mesoscopic transport process.

In this work, we show that a nontrivial phonon drag effect, termed “cooling by transverse heat current,” can emerge in four-terminal thermoelectric systems with two electrodes and two thermal (phonon) baths (can also be baths with other collective excitations, e.g., charge-density waves). Through the cooling by transverse heat current effect, we mean that one of the two electronic reservoirs (the source or the drain) can be cooled by passing a heat current between the two thermal baths. Note that, throughout this paper, the meanings of the words “transverse” and “longitudinal” should be interpreted through the configuration depicted Fig. 1. They refer rather to configurations instead of genuine geometry. Nevertheless, the configurations have geometric origins and may relate to

\*jianhua.jiang@suda.edu.cn

†Deceased.

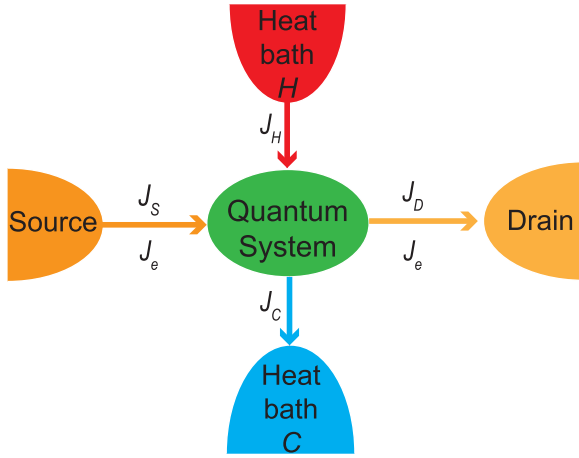


FIG. 1. Schematic of a four-terminal mesoscopic thermoelectric device. The source and the drain are electronic reservoirs. The other two terminals serve as the heat baths which only provide collective excitations to the central quantum system (i.e., provide only energy output or input). They do not exchange charge with the central quantum system nor other reservoirs. One heat bath  $H$  has higher temperature than the other heat bath  $C$ . These heat baths can be bosonic (e.g., phonon bath) or electronic (e.g., electronic bath with charge fluctuations as the collective excitations). Four heat currents  $J_S, J_H, J_C, J_D$  and the electric current  $J_e$  are illustrated.

a specific geometry in genuine material systems. The key microscopic processes are the inelastic transport assisted by the collective excitations in the thermal baths. The inelastic transport also yields other anomalous effects such as transverse thermoelectric effects (i.e., electrical current and power can be induced by a transverse temperature gradient). Here, the transverse thermoelectric effect is similar to the Nernst-Ettingshausen effect but not due to time-reversal symmetry broken by a magnetic field or magnetization, instead due to broken space symmetry (chirality). The cooling by transverse heat current is similar to the thermal Hall effect, which is again not due to broken time-reversal symmetry but rather to the inelastic transport and broken space symmetry. These unconventional transport effects are promising for heat control on the nanoscale as well as high-performance thermoelectric devices, as shown by our results. The spatial separation of heat and charge flow [3,8,26,38,43], as well as the enriched controllability enables more degrees of freedom to manipulate thermoelectric transport. In this work, we first discuss the linear thermoelectric transport and the thermoelectric figure of merit in the four-terminal inelastic thermoelectric systems. We then study the cooling by transverse heat current effect with emphasizing on the cooling efficiency and power beyond the linear transport regime. Last, we show that the four-terminal inelastic devices can realize a type of Maxwell demon using nonequilibrium baths.

This paper is organized as follows: Section II gives the basic thermodynamic framework for the study of thermoelectric transport. Specifically, the thermodynamic currents and affinities are given and the linear transport theory is established. Section III introduces the microscopic model and its realization using quantum-dots systems. Transport currents and the linear transport coefficients are derived. In Sec. IV,

we investigate the longitudinal (conventional) and transverse thermoelectric transport as well as their figures of merit. In Sec. V, we discuss in detail the effect of cooling by transverse heat current. In Sec. VI, we demonstrate the Maxwell demon in the four-terminal system. In Sec. VII, we study thermoelectric transport effects in quantum-dots ensembles. In Sec. VIII, we give the conclusions and discussions.

## II. THERMODYNAMIC CURRENTS AND AFFINITIES

We consider a four-terminal thermoelectric device as illustrated in Fig. 1. The electrical current  $J_e$  flows from source to drain. In addition, there are four heat currents,  $J_S, J_D, J_H$ , and  $J_C$ . Only three of them are independent, due to energy conservation, i.e.,

$$J_S + \frac{\mu_S}{e} J_e + J_H = J_C + J_D + \frac{\mu_D}{e} J_e, \quad (1)$$

where  $e$  is the carrier charge, and  $\mu_i$  ( $i = S, D$ ) are the electrochemical potentials of the two electrodes. The three independent heat currents are chosen as the heat current flowing out of the source  $J_S$ , and the symmetric and antisymmetric combinations of  $J_H$  and  $J_C$ , defined as

$$J_{\text{in}} \equiv J_H - J_C, \quad J_q \equiv \frac{J_H + J_C}{2}. \quad (2)$$

$J_{\text{in}}$  is regarded as the total heat current injected into the central quantum system from the two thermal baths, while  $J_q$  is the heat exchange current between the two heat baths intermediated by the central quantum system.

The affinities can be found via examining the entropy production,

$$\frac{dS}{dt} = -\frac{J_S}{T_S} - \frac{J_H}{T_H} + \frac{J_D}{T_D} + \frac{J_C}{T_C}, \quad (3)$$

where  $T_i$  ( $i = S, D, H, C$ ) are the temperatures of the four reservoirs. Inserting Eq. (1), we obtain

$$\begin{aligned} \frac{dS}{dt} &= J_S \left( \frac{1}{T_D} - \frac{1}{T_S} \right) + J_{\text{in}} \left( \frac{1}{T_D} - \frac{1}{2T_H} - \frac{1}{2T_C} \right) \\ &+ J_q \left( \frac{1}{T_C} - \frac{1}{T_H} \right) + J_e \left( \frac{\mu_S - \mu_D}{eT_D} \right) \end{aligned} \quad (4)$$

$$\equiv J_S A_S + J_{\text{in}} A_{\text{in}} + J_q A_q + J_e A_e. \quad (5)$$

Hence the affinities are

$$\begin{aligned} A_S &\equiv \frac{1}{T_D} - \frac{1}{T_S}, & A_{\text{in}} &\equiv \frac{1}{T_D} - \frac{1}{2T_H} - \frac{1}{2T_C}, \\ A_q &\equiv \frac{1}{T_C} - \frac{1}{T_H}, & A_e &\equiv \frac{\mu_S - \mu_D}{eT_D}. \end{aligned} \quad (6)$$

From the above, one can see that the heat current  $J_S$  is driven by the temperature difference between the source and the drain. In the linear-response regime,  $A_S \approx (T_S - T_D)/T^2$  where  $T$  is the equilibrium temperature of the whole system. On the other hand, the heat current  $J_{\text{in}}$  is driven by the temperature difference between the drain and the two heat baths. In the linear-response regime,  $A_{\text{in}} \approx (T_{\text{av}} - T_D)/T^2$  where  $T_{\text{av}} \equiv \frac{1}{2}(T_H + T_C)$  is the average temperature of the two heat baths. In comparison,  $J_q$  is driven by the temperature difference between the two heat baths, i.e., in linear response,  $A_q \approx (T_H - T_D)/T^2$ .

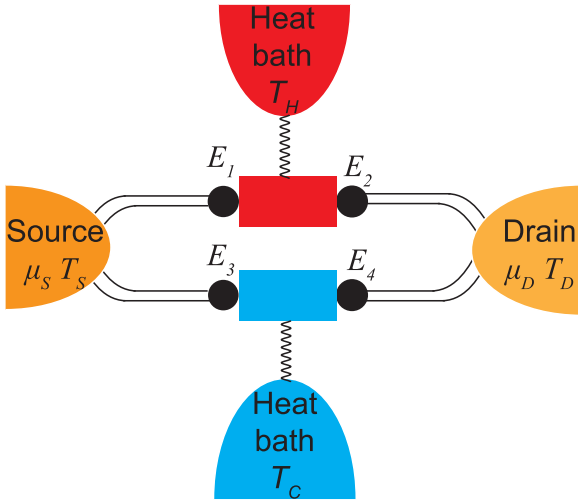


FIG. 2. Schematic of QD four-terminal thermoelectric devices. There are two parallel transport channels. Each channel has two QDs with different energies and a heat bath to enable inelastic transport. The two channels are spatially separated so that the heat bath  $H$  ( $C$ ) couples only to the upper (lower) channel.

### III. MICROSCOPIC SYSTEMS AND REALIZATIONS IN QUANTUM-DOT SYSTEMS

We consider the quantum-dot system illustrated in Fig. 2 and show that several unconventional phenomena can emerge. The system consists of four QDs: QDs 1 and 2 (of electronic energy  $E_1$  and  $E_2$ ) are coupled with the hot heat bath  $H$ , while QDs 3 and 4 (of energy  $E_3$  and  $E_4$ ) are coupled with the cold heat bath  $C$ . The two transport channels, QDs 1 and 2 vs QDs 3 and 4, are independent of each other. We first illustrate the underlying physics using QDs with a single energy level, and then extend the theory to the more realistic situations using QDs with many energy levels that obey the Gaussian distribution. Such a model with many energy levels describes many parallel copies of the microscopic system depicted in Fig. 2. We assume that the system is in the high-temperature regime (e.g.,  $\gtrsim 100$  K) where the phonon-assisted inelastic transport is dominant and the Coulomb interactions can be ignored without affecting the qualitative results and conclusions. Such a high-temperature regime is also advantageous for waste heat harvesting and cooling applications based on inelastic thermoelectric transport due to electron-phonon interactions. This is because the phonon density of states at the several tens of meV scale is significant and the phonon occupation numbers also increase with temperature. Meanwhile, the Coulomb interactions become less relevant because they are considerably weaker than other energy scales such as  $k_B T$  and the QD energies. To suppress the elastic sequential tunneling, we consider QDs with mismatched energies, i.e.,  $E_1 \neq E_2$  and  $E_3 \neq E_4$ . We focus on the regime where the energy differences  $|E_1 - E_2|$  and  $|E_3 - E_4|$  are comparable or larger than  $k_B T$ . We remark that, beside the phonon-assisted transport, there are several other mechanisms that can induce inelastic transport, such as charge fluctuations [25], photons [37,44], and magnons [45]. The relevant interactions in these mechanisms are the Coulomb interaction, the electron-photon interaction, and the exchange interaction, respectively. The

heat baths can be bosonic (e.g., phonon baths) or electronic (e.g., electrodes capacitively coupled with the central quantum system). On the other hand, the QDs can be replaced by quantum-wells [46] and  $p$ - $n$  junctions [26]. In all these realizations, the temperatures of the four reservoirs can be controlled by local heating. The substrate also affects the local temperatures of these reservoirs.

In the model considered in this work, the phonon-assisted hopping particle currents through the two independent channels are calculated as follows:

$$I_{12} = \Gamma_{1 \rightarrow 2} - \Gamma_{2 \rightarrow 1}, \quad I_{34} = \Gamma_{3 \rightarrow 4} - \Gamma_{4 \rightarrow 3}, \quad (7)$$

where  $\Gamma_{i \rightarrow j} = 2\gamma_{ep} f_i (1 - f_j) N_{ij}$  is the electron transfer rate from QD  $i$  to QD  $j$ . The prefactor 2 takes into account the spin degeneracy in electrons.  $\gamma_{ep}$  is the phonon-assisted hopping rate calculated from the Fermi golden rule. We remark that  $\gamma_{ep}$  is a parameter specific to material and system. It depends on the material that makes the QDs, as well as the substrate where the QDs reside. Besides, it depends on the geometry of QDs.  $\gamma_{ep}$  also depends on the phonon energy because it is related to the phonon density of states. We argue that  $\gamma_{ep}$  should be optimized for realistic systems to enhance the electron-phonon scattering rate so that the unconventional thermoelectric effects predicted in this work can be significant. However, because here we do not target specific materials but instead focus on the principles and mechanisms, for all calculations in this work, we have set  $\gamma_{ep} = 1$ . None of the results presented in the figures in this work depend on the specific number adopted for the parameter  $\gamma_{ep}$ .  $f_i$  is the electronic distribution on the  $i$ th QD ( $i = 1, 2, 3, 4$ ).  $N_{ij} \equiv |n_B(E_j - E_i)/k_B T_{ij}|$  where  $n_B \equiv 1/(e^x - 1)$  is the Bose-Einstein distribution function,  $T_{12} = T_{21} = T_H$  and  $T_{34} = T_{43} = T_C$ . In the above,  $I_{12}$  is the particle current flowing from the QD 1 to the QD 2,  $I_{34}$  is the particle current flowing from the QD 3 to the QD 4.

At the nonequilibrium steady states, the electronic distributions on the QDs,  $f_i$ , can be determined by the quantum master-equation approach. In this work, we shall instead consider the following simpler situations where the underlying physics can be revealed directly by using the Fermi golden rule (i.e., the rate equation) approach. For this purpose, we assume that the contacts between the source and the two QDs 1 and 3 can be made very good. Under such conditions, we can approximate the distributions on the two QDs 1 and 3 as  $f_1 \approx n_F(\frac{E_1 - \mu_S}{k_B T_S})$  and  $f_3 \approx n_F(\frac{E_3 - \mu_S}{k_B T_S})$ , where  $n_F \equiv 1/(e^x + 1)$  is the Fermi-Dirac distribution. Similarly, if the contacts between the drain and the two QDs 2 and 4 can be very good, the distributions on QDs 2 and 4 can be approximated as  $f_2 \approx n_F(\frac{E_2 - \mu_D}{k_B T_D})$  and  $f_4 \approx n_F(\frac{E_4 - \mu_D}{k_B T_D})$ .

When the linewidth of the QDs are much smaller than  $k_B T$ , we can ignore the linewidth of the QDs. In this regime, the relationships between the currents are

$$J_S = (E_1 - \mu_S)I_{12} + (E_3 - \mu_S)I_{34}, \quad (8a)$$

$$J_H = \omega_1 I_{12}, \quad J_C = -\omega_{-1} I_{34}, \quad (8b)$$

$$\omega_1 \equiv \omega_u \equiv E_2 - E_1, \quad \omega_{-1} \equiv \omega_d \equiv E_4 - E_3. \quad (8c)$$

From the definition of the heat currents, we have

$$J_{\text{in}} = \omega_1 I_{12} + \omega_{-1} I_{34}, \quad J_q = \frac{1}{2}(\omega_1 I_{12} - \omega_{-1} I_{34}). \quad (9)$$

Linear expansion of the currents in Eq. (7) in terms of the affinities, and using the above equations, we obtain the following linear-response transport equations:

$$J_i = \sum_j M_{i,j} A_j, \quad i, j = e, S, in, q \quad (10)$$

The physical transport coefficients are given by the matrix elements  $M_{i,j}$ . For instance, the electrical conductance is given by  $G = M_{e,e}T$ , while the diagonal heat conductances are  $K_S = M_{S,S}T$ ,  $K_{in,in} = M_{in,in}T$ , and  $K_{q,q} = M_{q,q}T$ . Microscopically, the transport coefficients are given by

$$M_{i,j} = \frac{\Gamma_0}{k_B} \langle a_i a_j \rangle, \quad (11)$$

$$a_e \equiv e, \quad a_S \equiv E_{l,\sigma} - \mu, \quad a_{in} \equiv \omega_\sigma, \quad a_q \equiv \frac{1}{2} \sigma \omega_\sigma. \quad (12)$$

Here,  $\Gamma_0 \equiv \Gamma_{1 \rightarrow 2}^0 + \Gamma_{3 \rightarrow 4}^0$  where the superscript 0 denotes the quantities calculated at thermal equilibrium.  $e$  is the elementary charge of the carrier. The average in the above equation is defined upon the two channels

$$\langle \dots \rangle = \sum_\sigma p_\sigma \dots \quad (13)$$

Here, the integer index  $\sigma$  is used to label the two channels:  $\sigma = 1$  for the upper channel and  $\sigma = -1$  for the lower channel. Thus,  $p_1 \equiv \Gamma_{1 \rightarrow 2}^0 / \Gamma_0$  for the upper channel, while  $p_{-1} \equiv \Gamma_{3 \rightarrow 4}^0 / \Gamma_0$  for the lower channel and  $\sum_\sigma p_\sigma = 1$ . Therefore, the weights for the average are proportional to the hopping rate in each channel.  $E_{l,\sigma}$  in Eq. (12) denotes the energy of the QD on the left side of each channel, i.e.,  $E_{l,1} = E_1$  for the upper channel and  $E_{l,-1} = E_3$  for the lower channel.  $\mu$  is the equilibrium chemical potential which is set as the energy zero throughout this paper, i.e.,

$$\mu \equiv 0. \quad (14)$$

$\omega_1$  and  $\omega_{-1}$ , as given in Eq. (8c), represent the energy difference between the QDs in the up and down channels, respectively.

#### IV. CONVENTIONAL AND UNCONVENTIONAL THERMOELECTRIC ENERGY CONVERSIONS

In the four-terminal system, there are three Seebeck coefficients

$$S_S = \frac{M_{e,S}}{M_{e,e}T} = \frac{k_B}{e} \frac{p_1 E_1 + p_{-1} E_3}{k_B T} = \frac{k_B}{e} \frac{\langle a_S \rangle}{k_B T}, \quad (15)$$

$$S_{in} = \frac{M_{e,in}}{M_{e,e}T} = \frac{k_B}{e} \frac{p_1 \omega_1 + p_{-1} \omega_{-1}}{k_B T} = \frac{k_B}{e} \frac{\langle a_{in} \rangle}{k_B T}, \quad (16)$$

$$S_q = \frac{M_{e,q}}{M_{e,e}T} = \frac{k_B}{e} \frac{p_1 \omega_1 - p_{-1} \omega_{-1}}{2k_B T} = \frac{k_B}{e} \frac{\langle a_q \rangle}{k_B T}. \quad (17)$$

Here, the average is defined in Eq. (13) and the quantities  $a_S$ ,  $a_{in}$ , and  $a_q$  are defined in Eq. (12). The above three Seebeck coefficients represent the thermoelectric effects induced by three temperature gradients corresponding to the three thermal affinities  $A_S$ ,  $A_{in}$ , and  $A_q$ . The first one is the conventional thermoelectric effect, the second one is the inelastic thermoelectric effect studied in Refs. [8,26,30,38], and the third one

is the transverse thermoelectric effect proposed and studied in this work. An important question is which symmetry needs to be broken to get the finite Seebeck coefficients given above. For example, a finite  $S_S$  needs the breaking of ‘‘particle-hole’’ symmetry,  $\mathcal{T}_{PH}$ , around the equilibrium chemical potential  $\mu$  [30]. A finite  $S_{in}$  is related to broken left-right mirror symmetry,  $\mathcal{T}_{Mx}$  [30]. From the above equations, both the left-right  $\mathcal{T}_{Mx}$  and up-down  $\mathcal{T}_{My}$  mirror symmetries need to be broken to have finite  $S_q$ . Interestingly,  $S_q$  is invariant under the multiplicative operator  $\mathcal{T}_I = \mathcal{T}_{Mx} * \mathcal{T}_{My}$  (we call  $\mathcal{T}_I$  the inversion operator), but  $S_q$  changes sign under each of the mirror operators. In geometry, the broken of the two mirror symmetries while preserving the inversion symmetry is associated with broken chirality. Therefore, we can conclude that the transverse Seebeck coefficient  $S_q$  is associated with broken chirality.

In the transverse thermoelectric effect, the spatial separation of the charge and heat currents is advantageous (as demonstrated by the results in this work) since the electrical and thermal conduction can be manipulated independently [8,26,43]. Explicitly, the maximal energy efficiency  $\eta_{max}$  and the figure of merit for the transverse thermoelectric effect  $Z_q T$  is

$$\eta_{max} = \eta_C \frac{\sqrt{Z_q T + 1} - 1}{\sqrt{Z_q T + 1} + 1}, \quad (18a)$$

$$Z_q T = \frac{M_{e,q}^2}{M_{e,e} M_{q,q} - M_{e,q}^2} = \frac{\langle a_q \rangle^2}{\langle a_q^2 \rangle - \langle a_q \rangle^2}, \quad (18b)$$

where  $\eta_C$  is the Carnot efficiency of the thermoelectric engine and  $a_q = \frac{1}{2} \sigma \omega_\sigma$ . The power factor is defined as  $P_q = G S_q^2$ . From Eq. (18b), we can see that a large figure of merit can be achieved when the average of  $a_q$  is large while the variance of  $a_q$  is small. Besides, the following two types of unwanted heat or charge conduction must be suppressed: (1) the heat conduction from  $H$  to  $C$  that does not contribute to thermoelectric conversion, (2) the charge conduction between the source and the drain due to elastic processes. The former phonon heat conduction can be reduced by, e.g., enhancing phonon scattering with random interfaces and disorders between the  $H$  and  $C$  heat baths (or using materials with low phonon heat conductivity). The latter charge conduction leads to Joule heating. This charge conduction due to elastic processes can be suppressed by increasing the energy difference between the two QDs in each channel, or by enhancing the inelastic processes via strong electron-phonon interactions (e.g., using III-V semiconductor QDs where the electron-phonon coupling is strong) and high temperature [8]. It has been shown in Refs. [8] and [38] that a proper energy difference between the QDs can suppress the elastic conduction effectively.

A configuration favoring the figure of merit and power factor for the transverse thermoelectric effect is to have  $\omega_u = -\omega_d$ , i.e., opposite energy difference for the up and down channels. We also notice that a configuration with ‘‘quadrupole-type’’ symmetry, i.e.,  $E_1 = -E_2 = -E_3 = E_4$ , can lead to  $S_S = S_{in} = 0$ , but  $S_q \neq 0$ . In comparison, a ‘‘dipole-type’’ configuration,  $E_1 = -E_2 = E_3 = -E_4$ , favors thermoelectric conversion through  $S_{in}$ , as has been shown in

Ref. [38]. The above symmetries can be explicitly seen from Eqs. (15)–(17).

The figures of merit for the other two thermoelectric effects can be written in terms of the averages over the microscopic quantities,

$$Z_S T = \frac{\langle a_S \rangle^2}{\langle a_S^2 \rangle - \langle a_S \rangle^2}, \quad a_S = E_l, \quad (19a)$$

$$Z_{in} T = \frac{\langle a_{in} \rangle^2}{\langle a_{in}^2 \rangle - \langle a_{in} \rangle^2}, \quad a_{in} = \omega_\sigma. \quad (19b)$$

We remark that the above equations also hold for the situations where there are multiple transport channels. For instance, in an ensemble of QD pairs where electrons transport in parallel in the ensemble. Examples of such configurations were studied in Ref. [38] and will also be presented in this paper. Furthermore, unlike the conventional thermoelectric figure of merit in Eq. (19a) that requires the small variance of the electron energy, which is challenging to realize [39], the inelastic thermoelectric figure of merit [Eq. (19b)] and the transverse thermoelectric figure of merit [Eq. (18b)] do not require the small variance of the electron energy. Instead, the small variance of the phonon energy is required to achieve high figure of merit for these unconventional thermoelectric effects. Therefore, these unconventional thermoelectric effects open alternative routes toward high thermoelectric figure of merits which may not be limited by the conventional challenges.

## V. COOLING BY TRANSVERSE HEAT CURRENT

We discover a mode of cooling in our system, i.e., cooling, say, the source by driving a heat current between the heat baths  $H$  and  $C$ , i.e., the cooling by transverse heat current effect. This is different from the previous “cooling by heating” effect where cooling is driven by a finite heat current injected into the quantum system. In the cooling by transverse heat current effect, heat injected into the quantum system is not necessary, since the driving force of the cooling is the energy exchange between the two heat baths via the central quantum system.

It is convenient to demonstrate the cooling by transverse heat current effect in the situations with

$$A_e = A_{in} = 0. \quad (20)$$

The two heat currents of concern are then given by [29,47]

$$J_S = M_{S,S} A_S + M_{S,q} A_q, \quad (21a)$$

$$J_q = M_{S,q} A_S + M_{q,q} A_q. \quad (21b)$$

Cooling by transverse heat current is to cool the source (i.e.,  $J_S > 0$  despite  $A_S < 0$ ) by a positive  $J_q$  (we assume  $T_H > T_C$ , i.e.,  $A_q > 0$ ). To have  $J_S > 0$  while  $A_S < 0$ , one needs

$$M_{S,q} > 0. \quad (22)$$

We propose to fulfill such a requirement via the following energy configuration:

$$E_1 = \varepsilon, \quad E_2 = \varepsilon + \omega, \quad E_3 = \varepsilon + \omega, \quad E_4 = \varepsilon, \quad (23)$$

for  $\varepsilon\omega > 0$ . We shall consider the case with both  $\varepsilon > 0$  and  $\omega > 0$ . The situation with both  $\varepsilon$  and  $\omega$  negative gives the same results. There are lots of other energy configurations that can realize cooling by the transverse heat current effect. Here we consider the above energy configuration to simplify our discussions. We remark that the cooling by transverse heat current effect can also cool the drain instead of the source. Nevertheless, in this work, we discuss only the cooling of the source to simplify the study.

We then focus on situations restricted by Eq. (20). The restriction  $A_{in} = 0$  establishes a relation between  $T_H$  and  $T_C$ , so only one of them is independent. We may regard  $T_H$  as an independent variable, whereas  $T_C$  is determined by

$$T_C = \left( \frac{2}{T_D} - \frac{1}{T_H} \right)^{-1}. \quad (24)$$

We set  $T_S < T_D$  and aim at cooling the source (i.e.,  $J_S > 0$ ) using  $J_q$  through the mesoscopic heat thermal current effect.

The coefficient of performance (COP) for the cooling by transverse heat current effect in our four-terminal system is given by [48,49]

$$\eta_{\text{COP}} = \frac{J_S}{J_q}. \quad (25)$$

Microscopically, the currents are

$$J_S = \varepsilon I_{12} + (\varepsilon + \omega) I_{34}, \quad J_q = \frac{1}{2} \omega (I_{12} + I_{34}). \quad (26)$$

In the cooling by transverse heat current effect, when  $A_e = A_{in} = 0$ , the entropy production of the system is

$$\frac{dS}{dt} = J_S A_S + J_q A_q. \quad (27)$$

Therefore, we have

$$\eta_{\text{COP}} = \left( T_S A_q - \frac{T_S}{J_q} \frac{dS}{dt} \right) \frac{T_D}{T_D - T_S}. \quad (28)$$

The reversible COP is

$$\eta_{\text{COP}}^{\text{rev}} = \left( \frac{T_S}{T_C} - \frac{T_S}{T_H} \right) \frac{T_D}{T_D - T_S} = -\frac{A_q}{A_S}. \quad (29)$$

Furthermore,

$$\frac{\eta_{\text{COP}}}{\eta_{\text{COP}}^{\text{rev}}} = \frac{-J_S A_S}{J_q A_q} = 1 - \frac{1}{J_q A_q} \frac{dS}{dt}. \quad (30)$$

The above relationship clearly demonstrates that the cooling of the source is driven by  $A_q$ . In other words, the negative entropy production associated with the cooling of the source,  $J_S A_S < 0$ , is compensated by the positive entropy production of  $J_q A_q$ , in agreement with Kedem and Caplan [50].

It is expected that at the reversible COP  $\eta_{\text{COP}}^{\text{rev}}$ , the cooling power vanishes, since the entropy production rate and the currents vanish [41,51]. In other situations,  $0 < \eta_{\text{COP}} < \eta_{\text{COP}}^{\text{rev}}$ . We shall keep the temperature of the drain  $T_D$  as fixed in the discussions below. In realistic situations,  $T_D$  can be set by the temperature of the substrate.

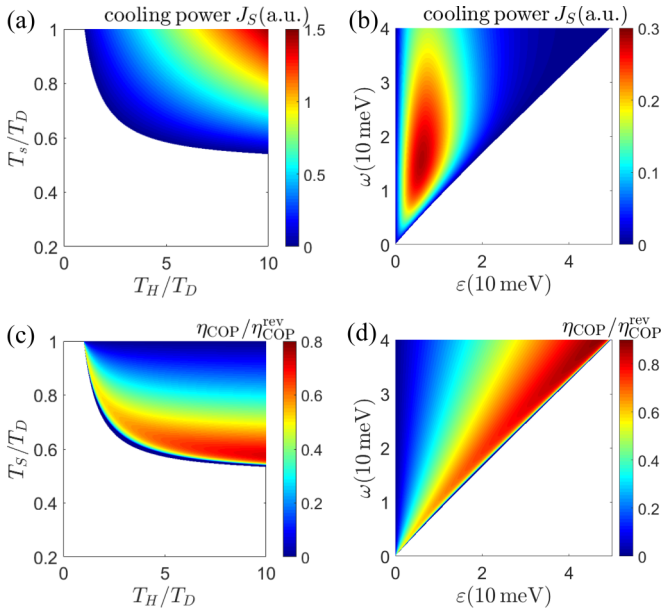


FIG. 3. (a) Cooling power  $J_S$  as functions of temperature ratios  $T_S/T_D$  and  $T_H/T_D$  for  $\varepsilon = 10$  meV and  $\omega = 20$  meV. (b) Cooling power  $J_S$  as functions of QD energies  $\varepsilon$  and  $\omega$  for  $k_B T_H = 60$  meV and  $k_B T_S = 6$  meV. (c) COP  $\eta_{\text{COP}}$  measured in units of the reversible COP  $\eta_{\text{COP}}^{\text{rev}}$  for the cooling by transverse heat current effect as a function of the temperature ratios  $T_S/T_D$  and  $T_H/T_D$  when QDs energy is the same as in panel (a). (d)  $\eta_{\text{COP}}^{\text{rev}}$  as functions of QD energies  $\varepsilon$  and  $\omega$  for the same parameters as in panel (b). Common parameters:  $\mu = 0$ ,  $k_B T_D = 10$  meV, and  $T_C = 1/(2/T_D - 1/T_H)$ . Throughout this paper, “a.u.” denotes “arbitrary units.”

The working condition of the cooling by transverse heat current effect is set by  $J_S > 0$  for  $A_S < 0$ . For each given energy configuration, this imposes restrictions on the temperatures  $T_H$  and  $T_S$ . In fact, there is a minimum temperature that one can cool the source down for a given set of  $T_H$  and  $T_S$ . On the other hand, for a given temperature of the source  $T_S$ , there is a minimum  $T_H$  to realize the cooling by the transverse heat current effect.

In Fig. 3(a), we plot the cooling power  $J_S$  as functions of the temperatures  $T_H$  and  $T_S$  measured in units of  $T_D$ . In the study in this section, we include the nonlinear effects in the transport by calculating the heat currents using the Fermi golden rule (i.e., the rate equation) approach [52]. As will be seen below, the cooling by transverse heat current effect is more visible in the large-temperature-bias regime. For a given set of  $\varepsilon$  and  $\omega$ , the cooling power increases with both  $T_H$  and  $T_S$ . The condition,  $J_S = 0$  defines the lowest temperature of the source  $T_S$  that can be cooled down for a given  $T_H$ , or the lowest temperature of the heat bath  $T_H$  that starts to cool the source via the thermal current effect at a given source temperature  $T_S$ . We use the Fermi golden rule, Eq. (7), to calculate the currents, power, and efficiency throughout this work.

In Fig. 3(b), we study the cooling power  $J_S$  as a function of  $\varepsilon$  and  $\omega$  for fixed  $T_S$  and  $T_H$ . The results provide useful information in the search of large cooling powers by tuning system parameters. It is found that high cooling powers can be achieved in the region with  $\omega \gg \varepsilon$ , especially for  $\omega < k_B T_H$ .

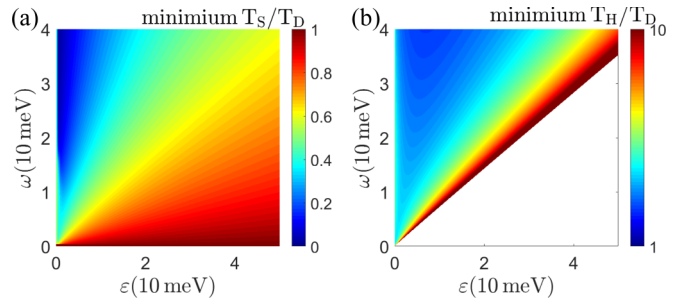


FIG. 4. (a) The lowest temperature of source  $T_S$  that can be cooled down via the cooling by transverse heat current effect as functions of  $\varepsilon$  and  $\omega$  for  $k_B T_H = 60$  meV. (b) The lowest temperature of the hot heat bath  $T_H$  that can perform the cooling by the transverse heat current effect as functions of  $\varepsilon$  and  $\omega$  for  $k_B T_S = 6$  meV and  $\omega \geq 0.9\varepsilon$ . Other parameters:  $\mu = 0$ ,  $k_B T_D = 10$  meV, and  $T_C = 1/(2/T_D - 1/T_H)$ .

In Fig. 3(c), we show the ratio of the COP over the reversible COP  $\eta_{\text{COP}}/\eta_{\text{COP}}^{\text{rev}}$  for a given energy configuration [ $\varepsilon = 10$  meV and  $\omega = 20$  meV, identical to Fig. 3(a)] as a function of the temperature ratios  $T_S$  and  $T_H$ . It is found that high ratios of  $\eta_{\text{COP}}/\eta_{\text{COP}}^{\text{rev}}$  appear for low  $T_S$  for a given  $T_H$ . In those regions, the cooling power is very small. In fact, the cooling power is large when  $T_S$  is high, i.e., the opposite trend of the COP. Such power-efficiency trade-off is consistent with existing knowledge (particularly as illustrated in Ref. [51] and later confirmed in Refs. [53] and [54]). The optimal ratio  $\eta_{\text{COP}}/\eta_{\text{COP}}^{\text{rev}}$  emerges close to the minimum  $T_S$  for the cooling by the transverse heat current effect.

The dependence of the ratio  $\eta_{\text{COP}}/\eta_{\text{COP}}^{\text{rev}}$  on the QD energy  $\omega$  and  $\varepsilon$  [for the same parameters as in Fig. 3(b)] is shown in Fig. 3(d). Large ratios of  $\eta_{\text{COP}}/\eta_{\text{COP}}^{\text{rev}}$  appear close to the minimum of  $\omega$  for each given  $\varepsilon$ . Apparently, the efficiency has an opposite trend in the dependence of QD energies. That is, the cooling power  $J_S$  is large for  $\omega \gg \varepsilon$ , while the COP ratio  $\eta_{\text{COP}}/\eta_{\text{COP}}^{\text{rev}}$  is large for  $\omega \approx \varepsilon$ .

We then study the optimal energy configuration,  $\omega$  and  $\varepsilon$ , that achieves the lowest temperature of the source  $T_S$  after a sufficiently long time cooling. This is determined by the lowest temperature of the source  $T_S$  that gives  $J_S = 0$ . The results are presented in Fig. 4(a). Again, the lowest  $T_S$  is achieved when  $\omega \gg \varepsilon$ . In the opposite limit,  $\varepsilon \gg \omega$ , the cooling by transverse heat current effect is quite ineffective. We also calculate the minimum temperature of the hot heat bath  $T_H$  required by cooling by the transverse heat current effect, i.e.,  $J_S = 0$ , for various energy configurations, as presented in Fig. 4(b). We find that the region with  $\omega \gg \varepsilon$  does not require too high a temperature of the heat bath  $T_H$  to perform cooling by transverse heat current. Therefore, a favorable parameter regime for cooling by the transverse heat current effect is  $\omega \gg \varepsilon$  with  $\omega \lesssim k_B T_H$ .

In realistic situations, the two energies  $\omega_u$  and  $\omega_d$  may not be equal. We show how the cooling power and COP vary with the two energies  $\omega_u$  and  $\omega_d$  in Fig. 5. Both the COP and the cooling power favor the situations with  $-\omega_u > \omega_d$ . For such a regime, cooling induced by the cold terminal  $C$  is more effective, since each phonon emission process gives more energy to the heat bath  $C$ . The entire picture is that the current

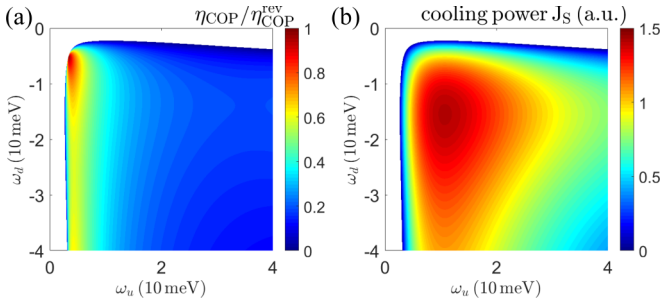


FIG. 5. (a) COP and (b) cooling power of cooling by the transverse heat current effect as functions the two energies  $\omega_u$  and  $\omega_d$ . Other parameters:  $\mu = 0$ ,  $k_B T_D = 10$  meV,  $k_B T_H = 15$  meV,  $E_1 = E_4 = 10$  meV, and  $T_C = 1/(2/T_D - 1/T_H)$ .

in the upper circuit  $I_{12}$  is sensitive to phonon temperature  $T_H$  and energy  $\omega_u$  since it is dominated by the thermal emission of phonons from the heat bath  $H$ . However, for the current in the lower circuit  $I_{34}$ , it is mostly determined by the temperature of the source and the drain, while relatively insensitive to the phonon temperature  $T_C$  and the energy  $\omega_d$ .

## VI. FOUR-TERMINAL SYSTEMS AS A MAXWELL DEMON

The second law of thermodynamics is a general law for macroscopic systems which states that the entropy production rate of any macroscopic system cannot be negative. An imagined system with feedback control that violates the conventional formulation of the second law was created by James C. Maxwell [55], which proposed that a creature (called “the Maxwell demon”) with the ability of tracking the velocity of individual gas particles could create a temperature gradient in two macroscopic chambers of gases which are originally at equilibrium with each other. The Maxwell demon can acquire and store the information of the particles. Removing such information, however, as revealed by Landauer [56], necessarily yields positive entropy production to restore the second law of thermodynamics. There have been a number of proposals of the Maxwell demon in different forms in various systems [57–62].

In this section, we study a possible implementation of the Maxwell demon in the quantum-dot architecture acting on a system without changing its number of particles or its energy, following the recent works [61,62] but in different setups and mechanisms. In the four-terminal setup illustrated in Fig. 6, our target is to induce a Maxwell demon based on two nonequilibrium baths (the cold and the hot baths) which can reduce the entropy of the system, the source and the drain, without giving energy or changing the particle number of the system. More explicitly, we aim to induce a heat flow from the cold reservoir, i.e., the source, to the hot reservoir, i.e., the drain, without exchanging energy or particle number with the system (i.e., the source plus the drain). This aim can be achieved by the cooling by transverse heat current effect at  $T_S < T_D$ . The entropy reduction in the source and drain is compensated by the larger entropy increase in the cold and hot heat baths. Therefore, the entropy increase rate of the whole

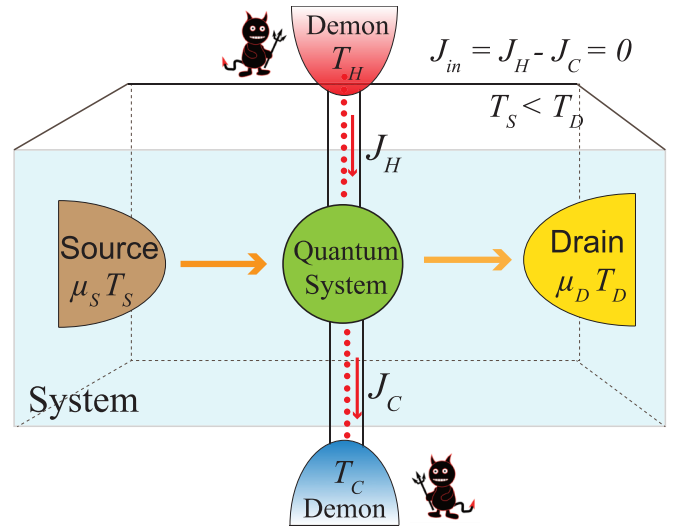


FIG. 6. Schematic of a four-terminal mesoscopic thermoelectric device as a Maxwell demon. The demon supplies no work or heat to the system, i.e., the total heat current injected into the central quantum system from the two thermal baths is zero,  $J_{in} = J_H - J_C = 0$ .

system is not negative and the second law of thermodynamics is not violated.

The condition for which the Maxwell demon neither injects nor extracts heat or energy is

$$J_{in} = 0. \quad (31)$$

Such an unconventional effect is driven by the temperature gradient between the two heat baths  $H$  and  $C$ . Therefore, the power of the Maxwell demon vanishes when the temperature gradient between the two heat baths  $H$  and  $C$  becomes zero.

We first show that the cooling by transverse heat current effect indeed survives even when  $J_{in} = 0$  (i.e., the total heat current injected into the quantum system is zero). In Fig. 7(a), we give the three thermal currents  $J_S$ ,  $J_q$ , and  $J_{in}$  as functions of  $\omega_d$  with other parameters fixed and given in the caption of the figure. We focus on the conditions where  $A_S < 0$ ,  $A_{in} = 0$ , and  $A_q > 0$ . It is seen from Fig. 7(a) that there is indeed a special point,  $\omega_d \simeq 57$  meV, where cooling by the transverse heat current effect survives at  $J_{in} = 0$ . We also notice from the figure that the sign change of  $J_{in}$  does not affect cooling by the transverse heat current effect. The COP  $\eta_{COP}$  and the cooling power  $J_S$  remain positive for  $\omega_d > 57$  meV, regardless of the sign change of the heat current  $J_{in}$ . However, only the case with  $J_{in} = 0$  represents the nonequilibrium Maxwell demon. In Fig. 7(b), we give the entropy production rate  $dS/dt$  and the COP ratio  $\eta_{COP}/\eta_{COP}^{rev}$  as functions of the energy  $\omega_d$ . It is seen that, as the entropy production rate decreases, the COP approaches  $0.83\eta_{COP}^{rev}$ . To visualize the energy conversion, we present the numerator and the denominator in Eq. (30), i.e.,  $-J_S A_S$  and  $J_q A_q$ , in Fig. 7(c). We further show the  $J_q A_q$  and the ratio  $\eta_{COP}/\eta_{COP}^{rev}$  in Fig. 7(d). Using log scales in these figures, one can see that, although the entropy production rate  $dS/dt$  is reducing with  $\omega_d$ , it is not vanishing even for large  $\omega_d$ . In fact, all the quantities,  $-J_S A_S$ ,  $J_q A_q$ , and  $dS/dt$ , are decreasing rapidly with increasing  $\omega_d$ , and there are visible discrepancies

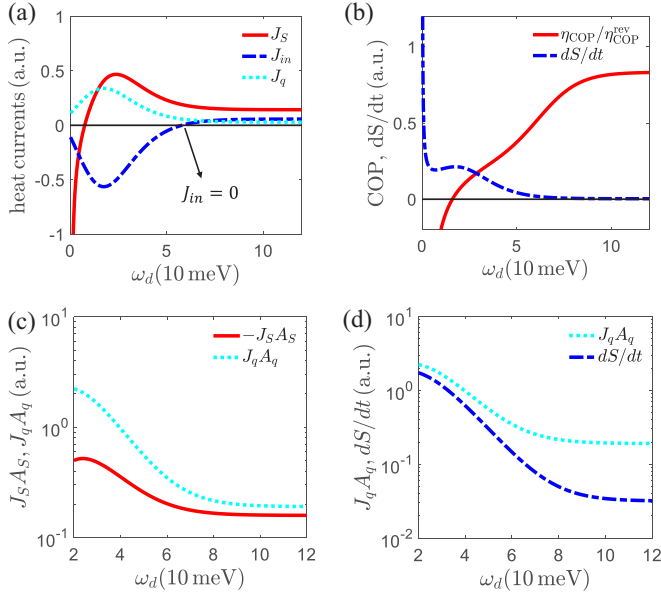


FIG. 7. (a) Thermal currents and (b) COP ratio  $\eta_{\text{COP}}/\eta_{\text{COP}}^{\text{rev}}$  and entropy production  $dS/dt$  as a function of QD energy  $\omega_d$ . (c)  $-J_S A_S$ ,  $J_q A_q$ , and (d)  $J_q A_q$ ,  $dS/dt$  as functions of QD energy  $\omega_d$ , where the y axis is in log scales. Other parameters:  $\mu = 0$ ,  $k_B T_D = 10$  meV,  $k_B T_H = 15$  meV,  $k_B T_S = 9$  meV,  $E_1 = E_4 = 10$  meV,  $\omega_u = 4$  meV, and  $T_C = 1/(2/T_D - 1/T_H)$ .

between the numerator  $-J_S A_S$  and the denominator  $J_q A_q$  in Eq. (30). In the end, as shown in Fig. 7(d), at large  $\omega_d$  the entropy production rate is still about 17% of the input  $J_q A_q$ . Therefore, the efficiency  $\eta_{\text{COP}}$  is about 83% of the reversible efficiency  $\eta_{\text{COP}}^{\text{rev}}$ .

Figure 8 presents the cooling power  $J_S$  and the COP as functions of the QD energies  $\omega_u$  and  $\omega_d$  at the condition  $J_{\text{in}} = 0$ . The white areas represent the parameter regions where the nonequilibrium Maxwell demon cannot be achieved. As shown in Fig. 8(a), high cooling powers can be achieved in the region with  $\omega_u < 10$  meV. However, in such a region, the cooling efficiency is small. In fact, Fig. 8(b) shows that the cooling efficiency is large only when  $\omega_u > 10$  meV, reflecting the power-efficiency trade-off in the nonequilibrium Maxwell demon mode [51,53].

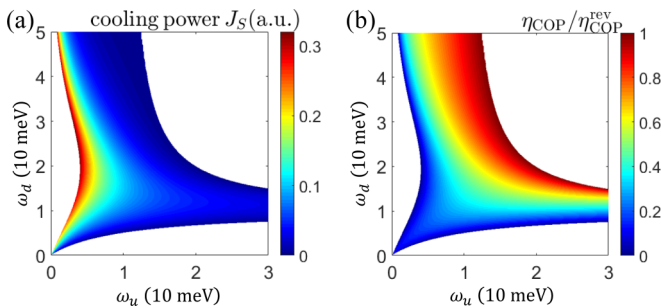


FIG. 8. (a) Cooling power  $J_S$  and (b) COP ratio  $\eta_{\text{COP}}/\eta_{\text{COP}}^{\text{rev}}$  of cooling by the transverse heat current effect as functions of the two energies  $\omega_u$  and  $\omega_d$  for  $J_{\text{in}} = 0$ . Other parameters:  $\mu = 0$ ,  $k_B T_D = 10$  meV,  $k_B T_H = 25$  meV,  $E_1 = E_4 = 10$  meV, and  $T_C = 1/(2/T_D - 1/T_H)$ .

## VII. THERMOELECTRIC TRANSPORT EFFECTS IN QUANTUM-DOT ENSEMBLES

To further study the performance of the thermoelectric and the cooling by the transverse heat current effects, we investigate the thermoelectric transport in quantum-dot ensembles. We consider the situations where there are multiple QDs pairs in the upper and lower channels in Fig. 2. For simplicity, we assume that electrons transport in parallel in these QDs pairs. The total transport effect can be calculated by summing up the currents in all possible channels. This model also describes electron transport in QDs with multiple energy levels. To simplify the problem, we use a distribution function to characterize the possible QD energy in the ensemble. Specifically, we consider the situations with Gaussian distributions of the QD energies. For instance, the Gaussian distributions of the QD energy  $E_i$  ( $i = 1, 2, 3, 4$ ) with a variance  $\Delta_{\text{QD}}^2$  are [38]

$$g_i(E_i) = \frac{\rho_0}{\Delta_{\text{QD}}\sqrt{2\pi}} \exp\left(-\frac{(E_i - E_{i0})^2}{2\Delta_{\text{QD}}^2}\right). \quad (32)$$

Here,  $\rho_0$  is related to the density of QDs in the ensemble. Generalizing the considerations in Sec. III, we obtain

$$J_e = \iint dE_1 dE_2 g_1(E_1) g_2(E_2) I_{12}(E_1, E_2) + \iint dE_3 dE_4 g_3(E_3) g_4(E_4) I_{34}(E_3, E_4). \quad (33)$$

Meanwhile we can get the expression of the heat current flowing out of the source:

$$J_S = \iint dE_1 dE_2 E_1 g_1(E_1) g_2(E_2) I_{12}(E_1, E_2) + \iint dE_3 dE_4 E_3 g_3(E_3) g_4(E_4) I_{34}(E_3, E_4), \quad (34)$$

and the heat exchange current between the two heat baths intermediated by the central quantum system is

$$J_q = \frac{1}{2} \iint dE_1 dE_2 (E_2 - E_1) g_1(E_1) g_2(E_2) I_{12}(E_1, E_2) - \frac{1}{2} \iint dE_3 dE_4 (E_4 - E_3) g_3(E_3) g_4(E_4) I_{34}(E_3, E_4). \quad (35)$$

The total heat current injected into the central quantum system from the two thermal baths is

$$J_{\text{in}} = \iint dE_1 dE_2 (E_2 - E_1) g_1(E_1) g_2(E_2) I_{12}(E_1, E_2) + \iint dE_3 dE_4 (E_4 - E_3) g_3(E_3) g_4(E_4) I_{34}(E_3, E_4). \quad (36)$$

In the above,

$$I_{12}(E_1, E_2) = \Gamma_{1 \rightarrow 2}(E_1, E_2) - \Gamma_{2 \rightarrow 1}(E_1, E_2), \quad (37a)$$

$$I_{34}(E_3, E_4) = \Gamma_{3 \rightarrow 4}(E_3, E_4) - \Gamma_{4 \rightarrow 3}(E_3, E_4). \quad (37b)$$

Here,  $\Gamma_{1 \rightarrow 2}(E_1, E_2) = 2\gamma_{ep} f_1(1 - f_2) N_{12}$  where  $f_1 = 1/\{\exp[(E_1 - \mu_S)/k_B T_S] + 1\}$ ,  $f_2 = 1/\{\exp[(E_2 - \mu_D)/k_B T_D] + 1\}$  and  $N_{12} = |1/\{\exp[(E_2 - E_1)/k_B T_H] - 1\}|$ . Similarly,

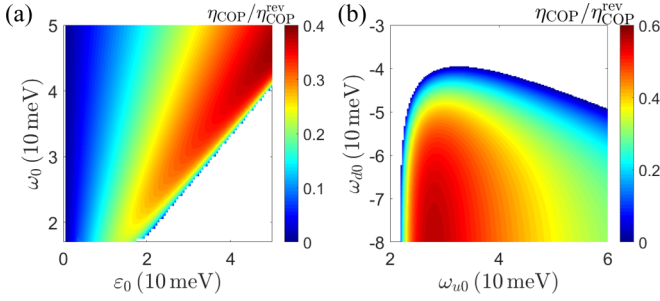


FIG. 9. (a) The COP ratio  $\eta_{\text{COP}}/\eta_{\text{COP}}^{\text{rev}}$  as functions of  $\omega_0$  and  $\epsilon_0$  for  $k_B T_H = 60$  meV. (b) COP ratio  $\eta_{\text{COP}}/\eta_{\text{COP}}^{\text{rev}}$  as functions the QD energies difference  $\omega_{u0}$  and  $\omega_{d0}$  when  $E_{10} = 10$  meV,  $E_{40} = 10$  meV,  $k_B T_H = 16$  meV. Other parameters:  $\mu = 0$ ,  $\Delta_{\text{QD}} = 2$  meV,  $k_B T_S = 6$  meV,  $k_B T_D = 10$  meV, and  $T_C = 1/(2/T_D - 1/T_H)$ . Note that  $\rho_0$  is irrelevant for the results here.

$\Gamma_{3 \rightarrow 4}(E_3, E_4) = 2\gamma_{ep}f_3(1 - f_4)N_{34}$  where  $f_3 = 1/\{\exp[(E_3 - \mu_S)/k_B T_S] + 1\}$ ,  $f_4 = 1/\{\exp[(E_4 - \mu_D)/k_B T_D] + 1\}$  and  $N_{34} = |1/\{\exp[(E_4 - E_3)/k_B T_C] - 1\}|$ . The linear transport coefficients can still be calculated using Eq. (11) where the average is now generalized to include the ensemble average defined by the distribution functions of the QD energies, i.e.,

$$\langle \dots \rangle = \iint dE_1 dE_2 \dots p_+(E_1, E_2) + \iint dE_3 dE_4 \dots p_-(E_3, E_4), \quad (38a)$$

$$p_+(E_1, E_2) = g_1(E_1)g_2(E_2)\Gamma_{1 \rightarrow 2}^0(E_1, E_2)/\mathcal{N}, \quad (38b)$$

$$p_-(E_3, E_4) = g_3(E_3)g_4(E_4)\Gamma_{3 \rightarrow 4}^0(E_3, E_4)/\mathcal{N}, \quad (38c)$$

$$\mathcal{N} = \iint dE_1 dE_2 g_1(E_1)g_2(E_2)\Gamma_{1 \rightarrow 2}^0(E_1, E_2) + \iint dE_3 dE_4 g_3(E_3)g_4(E_4)\Gamma_{3 \rightarrow 4}^0(E_3, E_4). \quad (38d)$$

In the above, the subscript  $+$  denotes the upper channel, while the subscript  $-$  denotes the lower channel (see illustration in Fig. 2).

We first study the cooling by the transverse heat current effect for the QD ensemble. In Fig. 9(a), we present the ratio of the COP over the reversible COP,  $\eta_{\text{COP}}/\eta_{\text{COP}}^{\text{rev}}$ , as a function of the QD energies  $\omega_0$  and  $\epsilon_0$  with the Gaussian distribution (here, we set  $E_{10} = E_{40} = \epsilon_0$ ,  $E_{20} = E_{30} = \omega_0 + \epsilon_0$ ). From the figure, we find that the high cooling efficiency can be achieved in the region with large  $\omega_0$  and  $\epsilon_0$ . In addition, we present in Fig. 9(b) the ratio  $\eta_{\text{COP}}/\eta_{\text{COP}}^{\text{rev}}$  as a function of the two energies  $\omega_{u0}$  and  $\omega_{d0}$  when  $E_{10} = 10$  meV and  $E_{40} = 10$  meV. We find that the cooling efficiency reaches the optimal value when  $15 \text{ meV} < \omega_{d0} < 20 \text{ meV}$ . By comparing Fig. 9(a) with Fig. 3(d), and Fig. 9(b) with Fig. 5(a), we find that for QD ensembles with a finite Gaussian broadening  $\Delta_{\text{QD}}$  in the QD ensemble leads to lower energy efficiency. But the qualitative features are the same.

We then study the cooling power  $J_S$  and the ratio  $\eta_{\text{COP}}/\eta_{\text{COP}}^{\text{rev}}$  as functions of the temperatures  $T_H$  and  $T_S$

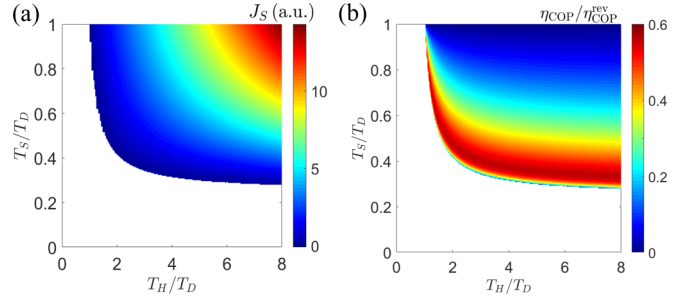


FIG. 10. (a) Cooling power  $J_S$ , (b) COP ratio  $\eta_{\text{COP}}/\eta_{\text{COP}}^{\text{rev}}$  as functions of temperature ratios  $T_S/T_D$  and  $T_H/T_D$ , the parameters are  $E_{10} = 10$  meV,  $E_{20} = 40$  meV,  $E_{30} = -5$  meV,  $E_{40} = 10$  meV,  $\Delta_{\text{QD}} = 2$  meV, and  $T_C = 1/(2/T_D - 1/T_H)$ . Note that  $\rho_0$  is irrelevant for the results here.

measured in units of  $T_D$  for a given energy configuration ( $E_{10} = 10$  meV,  $E_{20} = 40$  meV,  $E_{30} = -5$  meV,  $E_{40} = 10$  meV) in Fig. 10. We find that large cooling power appears for high  $T_S$  and  $T_H$ . However, in such a regime, the cooling efficiency  $\eta_{\text{COP}}/\eta_{\text{COP}}^{\text{rev}}$  is very small, reflecting the power-efficiency trade-off [51,53]. These results are qualitatively consistent with Figs. 3(a) and 3(c). The energy efficiency is smaller in Fig. 10(b) for the same parameters when compared with the results in Fig. 3(c).

In our four-terminal thermoelectric system, both the conventional thermoelectric effect [related to  $S_S$  in Eq. (15)] and the transverse thermoelectric effect [related to  $S_q$  in Eq. (17)] coexist. Since the maximal energy efficiency of the thermoelectric engine increases with the figure of merit, we compare the figure of merit for the conventional thermoelectric effect and the transverse thermoelectric effect. The results are presented in Figs. 11(a) and 11(b) for the transverse and conventional thermoelectric effects, respectively. From the figures we find that the figure of merit for the transverse thermoelectric effect  $Z_q T$  is prominent for  $\omega_{u0} \approx -\omega_{d0}$ , whereas the figure of merit for the conventional thermoelectric effect  $Z_S T$  is prominent for  $\omega_{u0} \approx \omega_{d0}$ . Nevertheless, it is clearly visible that in the same parameter region, the optimal  $Z_q T$  ( $\simeq 3$ ) is larger than the optimal  $Z_S T$  ( $\simeq 1.5$ ). The

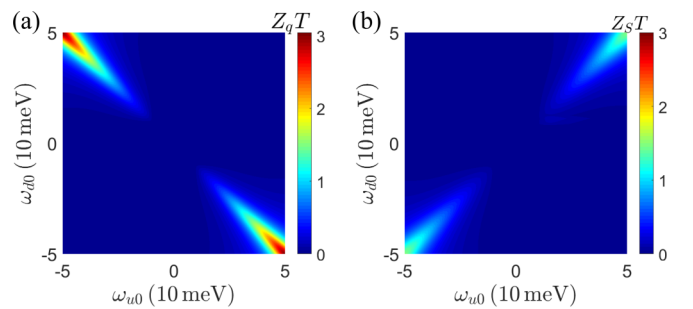


FIG. 11. (a) Figure of merit for the transverse thermoelectric effect  $Z_q T$  and (b) figure of merit for the conventional thermoelectric effect  $Z_S T$  as functions the QD energy differences  $\omega_{u0}$  and  $\omega_{d0}$  for the Gaussian distribution. Other parameters:  $\mu = 0$ ,  $k_B T = 10$  meV,  $\Delta_{\text{QD}} = 2$  meV,  $E_{10} + E_{20} = 0$ , and  $E_{30} + E_{40} = 0$ . Note that  $\rho_0$  is irrelevant for the results here.

results indicate that the transverse thermoelectric effect is potentially more advantageous than the conventional thermoelectric effect.

### VIII. CONCLUSION AND DISCUSSIONS

We have discovered and studied a mode of cooling by the transverse heat current effect, using a four-terminal (i.e., the source, the drain, and two thermal baths) QD thermoelectric device. Such an effect describes cooling of the source driven by the heat exchange between the two thermal baths, rather than the total heat injected into the quantum system [35]. A simple realization is to use a device with four QDs which simultaneously breaks the particle-hole symmetry, the left-right and up-down inversion symmetries. The cooling power and the energy efficiency manifest trade-off effect, e.g., high-energy efficiency comes with low cooling power, consistent with the common intuitions.

In addition, a transverse thermoelectric effect, i.e., generating electric power using the temperature difference between the two heat baths is studied. In the transverse thermoelectric effect, electric and heat transport are spatially separated. Such a thermoelectric effect has the advantage of manipulation of heat and charge transport in different spatial dimensions. Such spatial separation enables disentangling the correlations between electric conduction and phonon heat conduction, so that they can be engineered independently to yield high fig-

ure of merit and output power. The current-affinity relations, linear-transport properties, and the transverse thermoelectric figure of merit are studied.

We also show that the four-terminal quantum-dot system can realize a type of Maxwell demon where the demon exploits nonequilibrium effects to drag heat from a low-temperature reservoir (i.e., the source) to a high-temperature reservoir (i.e., the drain), even when there is no net energy and charge exchange between the demon and the system.

Finally, we generalize the transport equations to the situations with an ensemble of QDs pairs where electrons transport in parallel. We apply such a generalization for the study of energy efficiency for both the transverse thermoelectric effect and cooling by the transverse heat current effect. We find that the Gaussian broadening of QD energy leads to reduced energy efficiency. Our findings demonstrate that inelastic transport can bring about phenomena that have not been found in previous studies based on elastic transport processes as well as introduce alternative, promising routes toward high-efficiency thermoelectric energy conversions.

### ACKNOWLEDGMENTS

We acknowledge support from the National Natural Science Foundation of China (NSFC Grants No. 11675116 and No. 12074281), the Jiangsu distinguished professor funding and a Project Funded by the Priority Academic Program Development of Jiangsu Higher Education Institutions (PAPD).

- 
- [1] Y. Dubi and M. Di Ventra, Heat flow and thermoelectricity in atomic and molecular junctions, *Rev. Mod. Phys.* **83**, 131 (2011).
  - [2] B. Sothmann, R. Sánchez, and A. N. Jordan, Thermoelectric energy harvesting with quantum dots, *Nanotechnol.* **26**, 032001 (2015).
  - [3] J.-H. Jiang and Y. Imry, Linear and nonlinear mesoscopic thermoelectric transport with coupling with heat baths, *C. R. Phys.* **17**, 1047 (2016).
  - [4] H. Thierschmann, R. Sánchez, B. Sothmann, H. Buhmann, and L. W. Molenkamp, Thermoelectrics with Coulomb-coupled quantum dots, *C. R. Phys.* **17**, 1109 (2016).
  - [5] G. Benenti, G. Casati, K. Saito, and R. S. Whitney, Fundamental aspects of steady-state conversion of heat to work at the nanoscale, *Phys. Rep.* **694**, 1 (2017).
  - [6] R. Venkatasubramanian, E. Silvola, T. Colpitts, and B. O'Quinn, Thin-film thermoelectric devices with high room-temperature figures of merit, *Nature (London)* **413**, 597 (2001).
  - [7] D. Sánchez and R. López, Scattering Theory of Nonlinear Thermoelectric Transport, *Phys. Rev. Lett.* **110**, 026804 (2013).
  - [8] J.-H. Jiang, O. Entin-Wohlman, and Y. Imry, Thermoelectric three-terminal hopping transport through one-dimensional nanosystems, *Phys. Rev. B* **85**, 075412 (2012).
  - [9] G. Schaller, T. Krause, T. Brandes, and M. Esposito, Single-electron transistor strongly coupled to vibrations: Counting statistics and fluctuation theorem, *New J. Phys.* **15**, 033032 (2013).
  - [10] A. N. Jordan, B. Sothmann, R. Sánchez, and M. Büttiker, Powerful and efficient energy harvester with resonant-tunneling quantum dots, *Phys. Rev. B* **87**, 075312 (2013).
  - [11] D. Sánchez and L. Serra, Thermoelectric transport of mesoscopic conductors coupled to voltage and thermal probes, *Phys. Rev. B* **84**, 201307(R) (2011).
  - [12] R. Sánchez, B. Sothmann, and A. N. Jordan, Chiral Thermoelectrics with Quantum Hall Edge States, *Phys. Rev. Lett.* **114**, 146801 (2015).
  - [13] B. K. Agarwalla, J.-H. Jiang, and D. Segal, Full counting statistics of vibrationally assisted electronic conduction: Transport and fluctuations of thermoelectric efficiency, *Phys. Rev. B* **92**, 245418 (2015).
  - [14] H. Thierschmann, R. Sánchez, B. Sothmann, F. Arnold, C. Heyn, W. Hansen, H. Buhmann, and L. W. Molenkamp, Three-terminal energy harvester with coupled quantum dots, *Nat. Nanotechnol.* **10**, 854 (2015).
  - [15] B. K. Agarwalla, J.-H. Jiang, and D. Segal, Quantum efficiency bound for continuous heat engines coupled to noncanonical reservoirs, *Phys. Rev. B* **96**, 104304 (2017).
  - [16] A. Mu, B. K. Agarwalla, G. Schaller, and D. Segal, Qubit absorption refrigerator at strong coupling, *New J. Phys.* **19**, 123034 (2017).
  - [17] J. Lu, F. Zhuo, Z. Z. Sun, and J. H. Jiang, Cooperative spin caloritronic devices, *ES Energy Environ.* **7**, 17 (2019).
  - [18] G. Jaliel, R. K. Puddy, R. Sánchez, A. N. Jordan, B. Sothmann, I. Farrer, J. P. Griffiths, D. A. Ritchie, and C. G. Smith, Experimental Realization of a Quantum Dot Energy Harvester, *Phys. Rev. Lett.* **123**, 117701 (2019).

- [19] Y. Liu, R. Wang, J. Lu, C. Wang, and J.-H. Jiang, Energy cooperation in quantum thermoelectric systems with multiple electric currents, *Chin. Phys. B* **29**, 040504 (2020).
- [20] L. D. Hicks and M. S. Dresselhaus, Effect of quantum-well structures on the thermoelectric figure of merit, *Phys. Rev. B* **47**, 12727 (1993).
- [21] L. D. Hicks and M. S. Dresselhaus, Thermoelectric figure of merit of a one-dimensional conductor, *Phys. Rev. B* **47**, 16631 (1993).
- [22] R. Venkatasubramanian, Lattice thermal conductivity reduction and phonon localizationlike behavior in superlattice structures, *Phys. Rev. B* **61**, 3091 (2000).
- [23] K. Biswas, J. He, I. D. Blum, C. I. Wu, T. P. Hogan, D. N. Seidman, V. P. Dravid, and M. G. Kanatzidis, High-performance bulk thermoelectrics with all-scale hierarchical architectures, *Nature (London)* **489**, 414 (2012).
- [24] O. Entin-Wohlman, Y. Imry, and A. Aharony, Three-terminal thermoelectric transport through a molecular junction, *Phys. Rev. B* **82**, 115314 (2010).
- [25] R. Sánchez and M. Büttiker, Optimal energy quanta to current conversion, *Phys. Rev. B* **83**, 085428 (2011).
- [26] J.-H. Jiang, O. Entin-Wohlman, and Y. Imry, Three-terminal semiconductor junction thermoelectric devices: Improving performance, *New J. Phys.* **15**, 075021 (2013).
- [27] L. Simine and D. Segal, Vibrational cooling, heating, and instability in molecular conducting junctions: Full counting statistics analysis, *Phys. Chem. Chem. Phys.* **14**, 13820 (2012).
- [28] B. Sothmann, R. Sánchez, A. N. Jordan, and M. Büttiker, Rectification of thermal fluctuations in a chaotic cavity heat engine, *Phys. Rev. B* **85**, 205301 (2012).
- [29] J.-H. Jiang, O. Entin-Wohlman, and Y. Imry, Hopping thermoelectric transport in finite systems: Boundary effects, *Phys. Rev. B* **87**, 205420 (2013).
- [30] J.-H. Jiang, M. Kulkarni, D. Segal, and Y. Imry, Phonon thermoelectric transistors and rectifiers, *Phys. Rev. B* **92**, 045309 (2015).
- [31] L. Li and J.-H. Jiang, Staircase quantum dots configuration in nanowires for optimized thermoelectric power, *Sci. Rep.* **6**, 31974 (2016).
- [32] R. Wang, J. Lu, C. Wang, and J.-H. Jiang, Nonlinear effects for three-terminal heat engine and refrigerator, *Sci. Rep.* **8**, 2607 (2018).
- [33] J.-H. Jiang and Y. Imry, Near-field three-terminal thermoelectric heat engine, *Phys. Rev. B* **97**, 125422 (2018).
- [34] A. Mari and J. Eisert, Cooling by Heating: Very Hot Thermal Light can Significantly Cool Quantum Systems, *Phys. Rev. Lett.* **108**, 120602 (2012).
- [35] B. Cleuren, B. Rutten, and C. Van den Broeck, Cooling by Heating: Refrigeration Powered by Photons, *Phys. Rev. Lett.* **108**, 120603 (2012).
- [36] R. Härtle, C. Schinabeck, M. Kulkarni, D. Gelbwaser-Klimovsky, M. Thoss, and U. Peskin, Cooling by heating in nonequilibrium nanosystems, *Phys. Rev. B* **98**, 081404(R) (2018).
- [37] J. Lu, R. Wang, J. Ren, M. Kulkarni, and J.-H. Jiang, Quantum-dot circuit-QED thermoelectric diodes and transistors, *Phys. Rev. B* **99**, 035129 (2019).
- [38] J.-H. Jiang, Enhancing efficiency and power of quantum-dots resonant tunneling thermoelectrics in three-terminal geometry by cooperative effects, *J. Appl. Phys.* **116**, 194303 (2014).
- [39] G. D. Mahan and J. O. Sofo, The best thermoelectric, *Proc. Natl. Acad. Sci. USA* **93**, 7436 (1996).
- [40] J. Zhou, R. Yang, G. Chen, and M. S. Dresselhaus, Optimal Bandwidth for High Efficiency Thermoelectrics, *Phys. Rev. Lett.* **107**, 226601 (2011).
- [41] O. Entin-Wohlman, J.-H. Jiang, and Y. Imry, Efficiency and dissipation in a two-terminal thermoelectric junction, emphasizing small dissipation, *Phys. Rev. E* **89**, 012123 (2014).
- [42] R. S. Whitney, R. Sánchez, F. Haupt, and J. Splettstoesser, Thermoelectricity without absorbing energy from the heat sources, *Phys. E (Amsterdam, Neth.)* **75**, 257 (2016).
- [43] F. Mazza, S. Valentini, R. Bosisio, G. Benenti, V. Giovannetti, R. Fazio, and F. Taddei, Separation of heat and charge currents for boosted thermoelectric conversion, *Phys. Rev. B* **91**, 245435 (2015).
- [44] T. Ruokola and T. Ojanen, Theory of single-electron heat engines coupled to electromagnetic environments, *Phys. Rev. B* **86**, 035454 (2012).
- [45] B. Sothmann and M. Büttiker, Magnon-driven quantum-dot heat engine, *Europhys. Lett.* **99**, 27001 (2012).
- [46] B. Sothmann, R. Sánchez, A. N. Jordan, and M. Büttiker, Powerful energy harvester based on resonant-tunneling quantum wells, *New J. Phys.* **15**, 095021 (2013).
- [47] J.-H. Jiang, B. K. Agarwalla, and D. Segal, Efficiency Statistics and Bounds for Systems with Broken Time-Reversal Symmetry, *Phys. Rev. Lett.* **115**, 040601 (2015).
- [48] J. Lu, R. Wang, Y. Liu, and J.-H. Jiang, Thermoelectric cooperative effect in three-terminal elastic transport through a quantum dot, *J. Appl. Phys.* **122**, 044301 (2017).
- [49] J. Lu, Y. Liu, R. Wang, C. Wang, and J.-H. Jiang, Optimal efficiency and power, and their trade-off in three-terminal quantum thermoelectric engines with two output electric currents, *Phys. Rev. B* **100**, 115438 (2019).
- [50] O. Kedem and S. R. Caplan, Degree of coupling and its relation to efficiency of energy conversion, *Trans. Faraday Soc.* **61**, 1897 (1965).
- [51] J.-H. Jiang, Thermodynamic bounds and general properties of optimal efficiency and power in linear responses, *Phys. Rev. E* **90**, 042126 (2014).
- [52] J.-H. Jiang and Y. Imry, Enhancing Thermoelectric Performance using Nonlinear Transport Effects, *Phys. Rev. Appl.* **7**, 064001 (2017).
- [53] K. Proesmans, B. Cleuren, and C. Van den Broeck, Power-Efficiency-Dissipation Relations in Linear Thermodynamics, *Phys. Rev. Lett.* **116**, 220601 (2016).
- [54] K. Proesmans, Y. Dreher, M. Gavrilov, J. Bechhoefer, and C. Van den Broeck, Brownian Duet: A Novel Tale of Thermodynamic Efficiency, *Phys. Rev. X* **6**, 041010 (2016).
- [55] K. Maruyama, F. Nori, and V. Vedral, Colloquium: The physics of Maxwell's demon and information, *Rev. Mod. Phys.* **81**, 1 (2009).
- [56] R. Landauer, Irreversibility and heat generation in the computing process, *IBM J. Res. Dev.* **5**, 183 (1961).
- [57] M. D. Vidrighin, O. Dahlsten, M. Barbieri, M. S. Kim, V. Vedral, and I. A. Walmsley, Photonic Maxwell's Demon, *Phys. Rev. Lett.* **116**, 050401 (2016).
- [58] J. V. Koski, V. F. Maisi, T. Sagawa, and J. P. Pekola, Experimental Observation of the Role of Mutual Information in the Nonequilibrium Dynamics of a Maxwell Demon, *Phys. Rev. Lett.* **113**, 030601 (2014).

- [59] J. V. Koski, V. F. Maisi, J. P. Pekola, and D. V. Averin, Experimental realization of a Szilard engine with a single electron, *Proc. Natl. Acad. Sci. USA* **111**, 13786 (2014).
- [60] J. V. Koski, A. Kutvonen, I. M. Khaymovich, T. Ala-Nissila, and J. P. Pekola, On-chip Maxwell's Demon as an Information-Powered Refrigerator, *Phys. Rev. Lett.* **115**, 260602 (2015).
- [61] R. Sánchez, P. Samuelsson, and P. P. Potts, Autonomous conversion of information to work in quantum dots, *Phys. Rev. Research* **1**, 033066 (2019).
- [62] R. Sánchez, J. Splettstoesser, and R. S. Whitney, Nonequilibrium System as a Demon, *Phys. Rev. Lett.* **123**, 216801 (2019).